Development and Application of a Novel Microfabricated Device for the *In Situ* Tensile Testing of 1-D Nanomaterials

Yogeeswaran Ganesan, Yang Lu, Cheng Peng, Hao Lu, Roberto Ballarini, and Jun Lou

Abstract—We report on the development and application of a silicon microdevice for the *in situ* quantitative mechanical characterization of single 1-D nanomaterials within a scanning electron microscope equipped with a quantitative nanoindenter. The design makes it possible to convert a compressive nanoindentation force applied to a shuttle to uniaxial tension on a specimen attached to a sample stage. Finite-element analysis and experimental calibration have been employed to extract the specimen stress versus strain curve from the indentation load versus displacement curve. The stress versus strain curves for three 200–300-nm-diameter Ni nanowire specimens are presented and analyzed. [2009-0271]

Index Terms—*In situ*, microdevices, nanoindenter, nanomanipulation, nanomechanics.

I. Introduction

BECAUSE of their superior mechanical and electrical properties, 1-D nanomaterials such as metal and semiconductor nanowires and nanotubes have emerged as key components in a number of advanced and miniaturized electronic, optical, thermal, and electromechanical systems. The vast number of current and potential applications of these materials necessitates the need for a thorough understanding of their mechanical properties at comparable length scales due to their well-known size effects, i.e., the often-reported deviation from bulk properties at small scales. Their deformation behavior, in particular, is of great importance, since it affects the structural integrity and reliability of their parent systems. In addition to the technological driving force, these 1-D nanoscale entities provide unique opportunities and challenges toward the investigation of fundamental mechanisms in materials science, primarily those governing the origins of size-dependent mechanical behavior.

In situ nanomechanical testing provides a powerful means to study deformation processes and to observe the deformation mechanisms in nanomaterials through real-time imaging, for example, within a scanning electron microscope (SEM) chamber [1]. As a result, a considerable amount of attention has been focused on *in situ* experiments such as resonance-based tests [2], MEMS-based tensile testing [3], atomic-force-microscope (AFM)-assisted bending [4], compression [5] and tension tests [6], and tests conducted using electrostatically and thermally actuated platforms [7]–[10], among others, in order to probe the mechanical properties of nanomaterials and thin films. A number of the aforementioned techniques are either indirect (e.g., resonance-based testing), qualitative (e.g., AFM-assisted bending), or cannot be easily adapted for testing 1-D nanomaterials (e.g., the MEMS-based tensile testing technique for nanoscale thin films developed by Haque *et al.*). A major drawback with methods involving atomic force microscopy is that the force applied on and the deformation of the specimen cannot be simultaneously and independently measured. Furthermore, the force measurement is often semiquantitative at best, since it is based on an estimate of AFM probe stiffness and also because it relies on AFM tip deflection monitoring. The electrostatically and thermally actuated platforms developed by Espinosa *et al.* do overcome most of the limitations associated with some of the other aforementioned techniques. However, their technique relies on a complicated setup that involves separate microchips for sample loading and capacitance-based load measurement; its implementation is thus both expensive and challenging.

The device described in this paper was specifically designed to perform *in situ* quantitative tensile testing experiments on 1-D nanoscale building blocks, such as nanowires and nanotubes, within a SEM or transmission electron microscope (TEM) chamber equipped with a quantitative nanoindenter. Device actuation relies on a simple "push–pull" mechanism, as opposed to most of the existing techniques that involve electro- or thermomechanical coupling. Its simple design helps minimize the sources of errors, and the use of a quantitative nanoindenter helps overcome three of the main challenges associated with *in situ* experimental study of 1-D nanostructures, i.e., 1) application and measurement of forces with nano-Newton resolution; 2) measurement of local mechanical deformation with nanometer resolution; and 3) direct and independent measurement of load and deformation allowing real-time observation of the deforming samples.

Fig. 1. SEM images showing variations of the microdevice; devices labeled (a)–(d) belong to generation I, while devices labeled (e) and (f) belong to generation II. The devices labeled (a) and (f) are composed of inclined beams making a 60° angle with the sample-stage shuttles. The rest of the devices have inclined beams making a 45° angle with respect to the sample-stage shuttles.

II. DEVICE DESCRIPTION

A. Design

The devices used to perform the Ni nanowire tensile experiments described in this paper are one of the many (see Fig. 1) that were specifically designed for performing nanoscale tensile tests on 1-D nanomaterials within a SEM or TEM chamber equipped with a quantitative nanoindenter [11]. Load application (and measurement) and deformation measurement for the 1-D specimens are performed with the aid of the nanoindenter. The device consists of a pair of movable (sample-stage) shuttles that are attached to a top shuttle via inclined freestanding beams. Its actuation involves the usage of an *in situ* nanoindenter that applies a force on the top shuttle of the device along the y-axis (see Fig. 2). Four sets of inclined symmetrical beams transform the motion of the top shuttle into a 2-D translation of the sample-stage shuttles. Proper alignment of the nanoindenter head results in the sample-stage shuttles moving symmetrically along the y-axis and ensures that the load being applied across the sample, clamped between two ends of the sample-stage shuttles, is purely tensile. The force and displacement resolution of the devices are dictated by that of the nanoindenter and were ascertained via noise floor estimation experiments. The value for the displacement resolution was found to be equal to 0.8675 nm. The spring stiffness for the indenter was approximately 80 N/m (manufacturer specification). Hence, the load resolution was computed to be equal to 69.4 nN. With regard to stress versus strain curve extraction, the force on and elongation of the test specimen can be extracted from the nanoindenter load and tip displacement data via the following: 1) finite-element-analysis (FEA)-calculated conversion factors
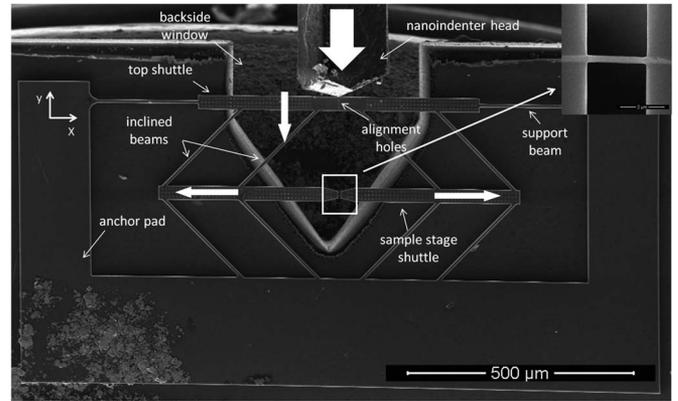

Fig. 2. SEM image of the microdevice and its components. The block arrows show the direction of the movement of the indenter tip and the shuttles during the experiment. (Inset) Close-up view of a nanowire sample.

or 2) energy balance. While the former technique, which is described in detail in this paper, was found to be primarily applicable for analyzing tests conducted on linear elastic (brittle) materials (the Ni nanowire specimens tested were found to be brittle materials), the latter technique would be suitable for more general materials and will be described in a future publication.

Device stiffness is dependent upon the thickness of the device layer, the number of support beams attached to the top shuttle, and the number and inclination angle of the inclined beams. Two separate sets of devices were fabricated using the procedure outlined in Fig. 3. The first set of devices, henceforth referred to as generation I devices, were fabricated on silicon-on-insulator (SOI) wafers having a device layer thickness of
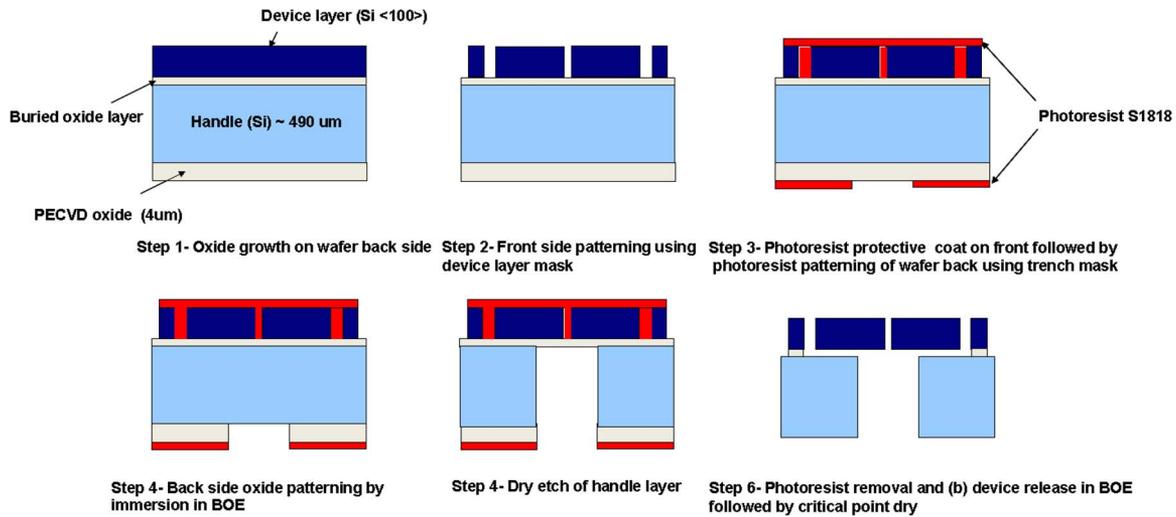
Fig. 3. Schematic shows the procedure adopted for microdevice fabrication. Note that the dimensions of the layers have not been drawn to scale.

9.5 ± 0.5 μm (see Fig. 1). For this generation of devices, the more compliant structures were composed of eight inclined beams at an angle of $45°$ with respect to the sample-stage shuttles. The stiffer structures had either eight inclined beams making a $60°$ angle or 20 inclined beams making a $45°$ angle with respect to the sample-stage shuttles. The second set of devices, henceforth referred to as generation II devices, were fabricated on SOI wafers having a device layer thickness of 6 ± 0.5 or 9 ± 0.5 μm. Each of these devices comprised eight inclined beams, each making an angle either $45°$ (more compliant) or $60°$ (stiffer) with respect to the sample-stage shuttles. The generation II devices also differed from the generation I ones with regard to the width of the shuttles, the separation between the inclined beams, and the shape of the sample-stage shuttles. Testing stage size is always a critical issue when setting up *in situ* nanomechanical characterization experiments within a TEM. The fabrication scheme adopted involved the use of dicing lines on the masks such that individual devices could be isolated from the wafers onto either 3 mm × 2 mm (generation I) or 2.5 mm × 1.2 mm (generation II) pieces. Also, an extended back-side window was incorporated into the design to facilitate nanoindenter head positioning and to ensure electron-beam transparency (a necessity for *in situ* TEM experiments).

B. Fabrication

As previously stated, the device fabrication process was tailored in order to obtain stand-alone devices with extended back-side windows. A similar scheme was adopted during the fabrication of both generations of devices, which is outlined in Fig. 3. The SOI wafers used during fabrication consisted of either a 9.5 ± 0.5-μm-thick Si $\langle 100 \rangle$ device layer, a 2-μm-thick buried oxide layer, and a 490 ± 10-μm-thick handle Si layer (generation I) or a 6 ± 0.5 μm/9 ± 0.5-μm-thick Si $\langle 100 \rangle$ device layer, a 5-μm-thick buried oxide layer, and a 490 ± 10-μm-thick handle Si layer (generation II). A bright field mask (device mask) was used for device patterning, while a dark field mask (trench mask) was employed to incorporate back-

side windows on the devices and for dicing lines to facilitate individual device isolation. First, a 4-μm-thick oxide film was grown on the back of the wafers by plasma-enhanced chemical vapor deposition at 340 °C, with SiH_4 and O_2 gases acting as the precursors. Standard photolithography techniques were then employed followed by a dry etching step, within a PlasmaTherm SLR-770 Inductively Coupled Plasma Reactive Ion Etcher (Plasma-Therm, St. Petersburg, FL) using the Bosch™ recipe, in order to pattern devices on the front side of the wafers. Subsequently, photolithographic techniques were again used to pattern dicing lines and windows on a resist layer coated on the back side of the wafer. Mask alignment, during this step, was performed using a SUSS MicroTec MA6 Mask Aligner (SUSS MicroTec AG, Garching, Germany) equipped with front-to-back alignment capability. The oxide layer on the back side of the wafer was then etched in a 10:1 buffered oxide etch (NH_4F:HF 36.2:4.7% by weight) solution. Before the sample was immersed into the buffered oxide etch solution, the front side of the wafer was coated with a thick photoresist layer in order to protect the exposed buried oxide layer. The handle layer was subsequently dry etched within the deep reactive ion etcher. The thick photoresist layer on the front side of the wafers was removed using acetone before device release, which involved the placement of the wafers in a buffered oxide etch tank for a specific amount of time. The duration of the release step was long enough for the movable portions of the device to be completely released while some of the oxide remained beneath the anchor pads, leaving them attached to the substrate. The samples were then placed in a methanol bath and subsequently dried within a supercritical drier (tousimis research corporation, Rockville, MD) using liquid carbon dioxide (in order to avoid stiction issues) before individual device isolation.

C. Data Analysis Using FEM Modeling

The details with regard to the FEA of the early version of devices and the associated testing procedure have been discussed earlier [12]. However, since the devices, the models, and the method for analysis of experimental data have been

modified considerably, the data analysis procedure using FEA is described in detail in the following. In order to derive the stress versus strain curve of the nanowire from the nanoindenter tip load versus displacement data, two parameters, namely, 1) the ratio of the force acting on the sample to the indenter tip applied load, i.e., the force conversion coefficient (C_F), and 2) the ratio of the sample-stage shuttle displacement/sample elongation to the nanoindenter tip displacement, i.e., the displacement conversion coefficient (C_D) must be determined. The values of C_F and C_D depend upon device stiffness and the stiffness of the specimen being tested (henceforth referred to as the sample stiffness). The sample stiffness can be estimated, using a finite-element model, from the system stiffness (K_s) defined as the ratio of the applied load to the displacement of the indenter tip, a parameter that can be ascertained from the experimental load versus displacement curve. The behavior of the device, clamped with a virtual nanowire sample, was modeled using ANSYS in order to generate three curves, namely, the system stiffness (K_s) versus sample stiffness curve [Fig. 4(a)], the force conversion coefficient (C_F) versus sample stiffness curve [Fig. 4(b)], and the displacement conversion coefficient (C_D) versus sample stiffness curve [Fig. 4(c)]. By interpolation of the latter two curves using the value of sample stiffness obtained from the first curve, the values of C_F and C_D for a given experiment were determined.

Because of the device's planar beam-based geometry, a 2-D FEA model was constructed using ANSYS Beam 32 elements. Material nonlinearities were ignored, since the device layer was made of single-crystal silicon, which is linear elastic at the temperatures at which the experiments were conducted. However, since large deformations might occur as the indenter load increases, geometry nonlinearities were considered in the analyses. For all the analyses, the Young's modulus and Poisson's ratio of single-crystal silicon ($\langle 100 \rangle$ orientation) were set equal to 160 GPa (obtained via nanoindentation of the device layer after fabrication) and 0.278, respectively [13]. Virtual nanowires (treated as ANSYS Link 1 elements) with a Poisson's ratio set equal to 0.310 (the value for nickel) [14] were used to model the device behavior in the presence of a sample.

III. DEVICE APPLICATION

A. Sample Positioning and Clamping

Sample positioning, in this case, refers to the placement of a 1-D nanomaterial at the desired location with micrometer resolution. The fact that the specimens must be freestanding, clamped at both ends, and well aligned in the tensile direction makes sample positioning and clamping quite a challenging task. The novel technique that was adopted in order to mount the Ni nanowires is thus described here in brief. A portion of each sample-stage shuttle was coated with a thin layer of epoxy (HARDMAN Water-Clear Epoxy). A droplet from a nickel nanowire solution, containing $\langle 112 \rangle$-oriented nanowires grown via electrodeposition [15], was first dispersed in isopropanol by ultrasonication for 5–10 min. A drop of this dispersion was deposited on top of a Si wafer coated with a 5-nm-thick layer of
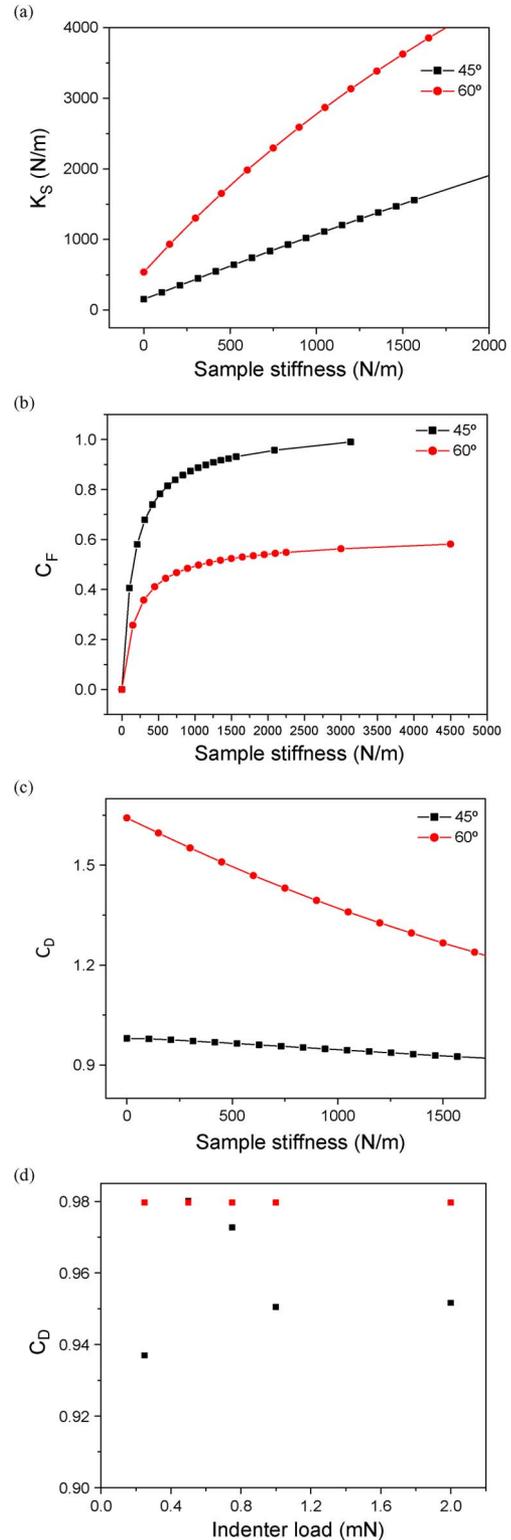

Fig. 4. (a) System stiffness K_s versus sample stiffness curves, (b) force conversion coefficient (C_F) versus sample stiffness curves, and (c) displacement conversion coefficient (C_D) versus sample stiffness curves, as obtained using FEA (the red and black curves correspond to 9 ± 0.5-μm-thick generation II devices that were composed of eight inclined beams making angles of $60°$ and $45°$ with respect to the sample-stage shuttles, respectively). (d) C_D plotted as a function of indenter load for a 9 ± 0.5-μm device [similar to the ones used in all the experiments reported in this paper; see Fig. 1(e)] in the absence of a mounted sample. The red points show the values of C_D, as obtained from FEA. The black points show the values of C_D obtained via analysis of SEM images captured during indentation.

titanium. Individual nanowires, $\sim 15\ \mu$m long and 200–300 nm in diameter and, hence, visible under an optical microscope, were subsequently picked up and placed across the shuttles using micromanipulators housed within a probe station (The Micromanipulator Company, Carson City, NV). Tungsten tips (The Micromanipulator Company, Carson City, NV) were used to perform the manipulation of the nanowires, since they were found to attach to the tips via electrostatic interaction. The epoxy layer, upon hardening, acts as a clamp for the tensile specimens.

B. Testing Procedure

The tensile experiment on the clamped nanowire was performed within a SEM (FEI Quanta 400 high-resolution field-emission SEM, FEI Company, Hillsboro, OR) equipped with an InSEM Indenter (Agilent Technologies, Oak Ridge, TN) system. A blunt cube corner nanoindenter tip was used to perform the indentation. $9 \pm 0.5\ \mu$m thick devices with eight $45°$ inclined beams attached to the sample-stage shuttles were used for all the experiments described in this paper [Fig. 1(e)]. The nanoindenter tip was first aligned with the top shuttle of the device in order to make sure that the sample-stage shuttles moved symmetrically. This was done with the help of alignment holes that had been incorporated in the device design. Once this was done, the electron beam was focused on the nanowire specimen in order to monitor its deformation as a function of load. The indentation was performed in the load-controlled mode, with the loading rate being held at a constant value of $\sim 30\ \mu$N/s (corresponds to a strain rate of approximately 0.007/s). The maximum load applied on the device was 2 mN. Once this value was reached, the load was held constant for 0.5 s; this was followed by an unloading step at the aforementioned rate. A thermal drift correction hold step was performed at 10% of the maximum applied load for about 50 s in order to account for small amounts of thermal expansion or contraction in the test material and/or indentation equipment.

C. Error Analysis

The technique outlined in this paper can be used to ascertain the value of the Young's modulus (E) of a 1-D nanomaterial using

$$E = \frac{\sigma}{\varepsilon} = \frac{F_x/A}{\Delta L/L} = \frac{C_F F_y L}{C_D y_1 A} \tag{1}$$

where C_F and C_D are, as stated previously, the force and displacement conversion coefficients, respectively; F_y is the force applied by the indenter; y_1 is the displacement of the top shuttle (assumed to be equal to the displacement of the nanoindenter head); and L and A are the sample length and cross-sectional

area, respectively. Thus, the uncertainty in the determination of the value of E, ΔE, can be computed using

$$(\Delta E)^2 = \left(\frac{\partial E}{\partial C_F}\right)^2 (\Delta C_F)^2$$

$$+ \left(\frac{\partial E}{\partial C_D}\right)^2 (\Delta C_D)^2 + \left(\frac{\partial E}{\partial F_y}\right)^2 (\Delta F_y)^2$$

$$+ \left(\frac{\partial E}{\partial y_1}\right)^2 (\Delta y_1)^2 + \left(\frac{\partial E}{\partial L}\right)^2 (\Delta L)^2$$

$$+ \left(\frac{\partial E}{\partial A}\right)^2 (\Delta A)^2$$

$$= E^2 \left(\left(\frac{\Delta C_F}{C_F}\right)^2 + \left(\frac{\Delta C_D}{C_D}\right)^2 + \left(\frac{\Delta F_y}{F_y}\right)^2 \right.$$

$$\left. + \left(\frac{\Delta y_1}{y_1}\right)^2 + \left(\frac{\Delta L}{L}\right)^2 + \left(\frac{\Delta A}{A}\right)^2 \right). \tag{2}$$

The relative uncertainty in the value of E can be expressed as (3), shown at the bottom of the page.

The uncertainties in the values of C_F and C_D arise from two sources, namely, random errors, such as variation of device thickness, and systematic errors, such as misalignment of indenter tip and/or specimen. The uncertainty in the value of C_F was estimated via FEA. For all the devices fabricated, the thickness variation was about $\pm 0.5\ \mu$m, the angles of indenter tip misalignment was assumed to be less than $5°$, the lateral misalignment of the indenter tip with respect to the center of the top shuttle was assumed to be less than $5\ \mu$m, and the angles of nanowire misalignment was assumed to be less than $10°$. The results of an error analysis conducted using FEA indicated that the error in the value of C_F, as a result of the aforementioned factors, would be less than 13% for a device with a mounted sample having a stiffness equal to 1500 N/m. In other words,

$$\Delta C_F / C_F = 13\%.$$

The error in the value of C_D was estimated by comparing the results of FEA with those obtained experimentally via indentation of a stand-alone device (device having no specimen attached to it). The values of C_D for the stand-alone device, in the load range of 0.25–2 mN, were obtained by loading it to preset levels, followed by acquisitions of high-resolution images of the sample-stage shuttle gap. The average experimental C_D value (0.96), when compared to the value obtained by FEA, yielded an error value of

$$\Delta C_D / C_D = 2\%.$$

$$\left| \frac{\Delta E}{E} \right| = \sqrt{ \left(\frac{\Delta C_F}{C_F}\right)^2 + \left(\frac{\Delta C_D}{C_D}\right)^2 + \left(\frac{\Delta F_y}{F_y}\right)^2 + \left(\frac{\Delta y_1}{y_1}\right)^2 + \left(\frac{\Delta L}{L}\right)^2 + \left(\frac{\Delta A}{A}\right)^2 } \tag{3}$$
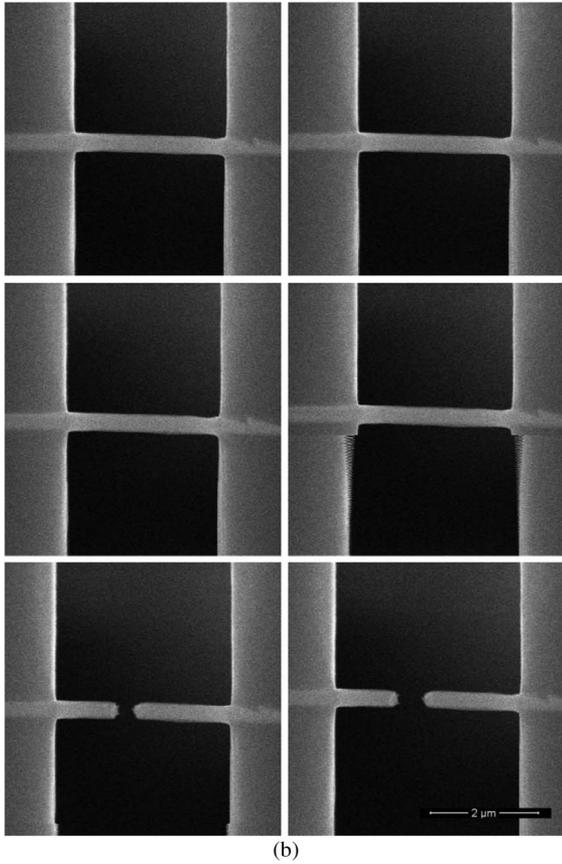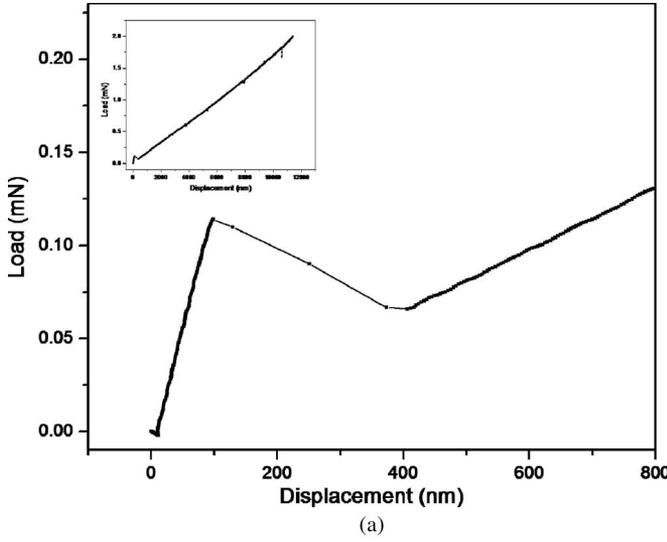
(a)

(b)

Fig. 5.   (a) Graph shows the nanoindenter load versus displacement curve for the first 7.5 s of an experiment performed on a 298-nm-diameter sample. The inset shows the load versus displacement curve for the entire loading part of the experiment. (b) SEM video snapshots show the aforementioned specimen during the tensile testing experiment.

The uncertainties in the measurement of force F_y and displacement y_1 arise mainly due to the precision of the nanoindenter. The force and displacement resolution values for the InSEM indenter are 69.4 nN and 0.8675 nm, respectively. The maximum force applied by the indenter and the maximum indenter head displacement (before sample failure) for a representative experiment conducted on a nickel nanowire
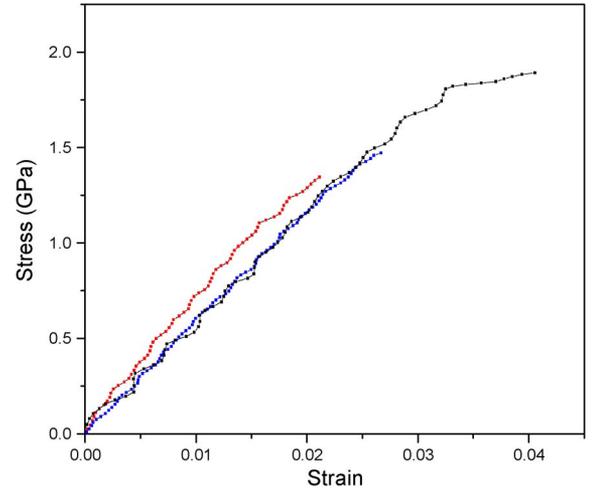

Fig. 6.   Engineering stress versus strain curves for the nanowire specimens (results summarized in Table I), as derived from the indenter load versus displacement data [see Fig. 5(a)]. The red curve corresponds to a 263-nm-diameter specimen, the blue curve corresponds to a 298-nm-diameter specimen, and the black curve corresponds to a 215-nm-diameter specimen.

were approximately 0.13 mN and 100 nm, respectively. Hence,

$$\left(\frac{\Delta F_y}{F_y}\right)^2 = \left(\frac{69.4 \text{ nN}}{0.13 \text{ mN}}\right)^2 < 1 \times 10^{-4}$$

$$\left(\frac{\Delta y_1}{y_1}\right)^2 = \left(\frac{0.8675 \text{ nm}}{100 \text{ nm}}\right)^2 < 1 \times 10^{-4}.$$

The uncertainties in the measurement of sample length and diameter arise from the pixel resolution of the SEM micrographs, which, in this case, is about 10 nm. Since the gauge length and diameter of the sample are on the order of 4 μm and 300 nm, respectively,

$$\left(\frac{\Delta L}{L}\right)^2 = \left(\frac{10 \text{ nm}}{4 \text{ }\mu\text{m}}\right)^2 < 1 \times 10^{-4}$$

$$\left(\frac{\Delta A}{A}\right)^2 = \left(\frac{2\Delta d}{d}\right)^2 = \left(\frac{2 \times 10 \text{ nm}}{300 \text{ nm}}\right)^2 = 4.4 \times 10^{-3}.$$

The value of the relative uncertainty (error) in the measurement of sample Young's modulus is thus about 14.73% (3). Clearly, the primary source of error is associated with the force conversion factor C_F and is produced by the uncertainties introduced by fabrication, sample manipulation, and the experimental setup.

IV. RESULTS AND DISCUSSION

The indenter load versus displacement curve for one of the three tests reported in this paper is shown in Fig. 5. The nickel nanowire specimen used for this experiment was about 12 μm long and had a diameter of 298 nm. The gauge length of the specimen, i.e., the distance between the clamping points, was ascertained by observation of the side profile of the sample across the sample-stage gap under a SEM and was found to be equal to 3.1 μm. The slope of the load versus displacement curve before and after sample failure was used to determine

TABLE I
TABLE SHOWS THE NANOWIRE PROPERTIES DETERMINED FROM THE STRESS–STRAIN CURVES SHOWN IN FIG. 6

Sample Diameter (nm)	Young's Modulus (GPa)	Ultimate tensile strength (GPa)	Failure strain (%)
298	56.879	1.472	2.66
215	55.556	1.896	4.0
263	62.993	1.35	2.11

the stiffness of the device in the presence of and after the failure of a mounted specimen. The initial slope of the curve (1259 N/m) corresponds to the stiffness of the device in the presence of the specimen before failure. A sudden change in the slope of the indentation curve occurs at a load value of about 0.114 mN, which is indicative of the nanowire sample failure. This phenomenon was independently verified from the sample deformation video. It occurs because, once the sample fails, the slope of the curve (155 N/m) must become equal to the stiffness of the device in the absence of a mounted sample, viz., 154.03 N/m as per the finite-element model [see Fig. 4(a)]. By interpolation, using the value of the slope before sample failure, of the system stiffness (K_s) versus sample stiffness curve [Fig. 4(a)], the sample stiffness was determined (1211 N/m). The values for C_F and C_D were subsequently determined [using the curves shown in Fig. 4(b) and (c)], and the stress versus strain curve (see Fig. 6) was plotted. The stress strain curves for two other samples were obtained in a similar fashion. One of the samples tested was found to have undergone small amount of plastic deformation (black curve in Fig. 6). In this case, two separate sets of values for C_F and C_D, obtained using two values of K_s, were used to derive the stress versus strain curve, since the obtained experimental curve clearly demonstrated bilinear features. The measured apparent Young's moduli (see Table I) for the Ni nanowire specimens from our experiments (equal to the slope of the stress versus strain curves shown in Fig. 6) were found to be about 25% of that of single-crystal Ni along the [112] direction, viz., 232.5 GPa [16]. Another feature that was revealed during the experiments was that the nanowires did not fracture until the value of applied stress reached a value greater than 1.3 GPa. The ultimate tensile strength values for the samples tested were found to be much higher than the ultimate tensile strength of Ni in bulk form, i.e., 140–195 MPa [17]. This phenomenon is attributed to the fact that when materials are scaled down, their strength approaches the theoretical strength, viz., approximately one-tenth of the Young's modulus [9].

V. CONCLUSION

As is evident from the previously described tests, the novel device and associated method outlined in this paper are convenient for carrying out tensile tests on 1-D nanomaterials such as metallic nanowires and nanotubes. The primary advantages of the technique are its simplicity and its capability to produce high-resolution quantitative data while enabling real-time observation of the sample deformation process. One must note that while the microdevice used for the experiments described

in this paper has been discussed in the context of *in situ* SEM tensile testing, a large number of related applications have been envisioned.

REFERENCES
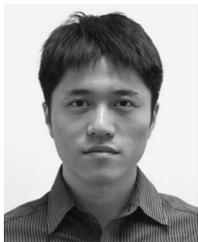
[1] F. Yang and J. C. M. Li, *Micro and Nano Mechanical Testing of Materials and Devices*. New York: Springer-Verlag, 2008, ch. 11.
[2] P. Poncharal, Z. L. Wang, D. Ugarte, and W. A. de Heer, "Electrostatic deflections and electromechanical resonances of carbon nanotubes," *Science*, vol. 283, no. 5407, pp. 1513–1516, Mar. 1999.
[3] M. A. Haque and M. T. A. Saif, "*In situ* tensile testing of nanoscale freestanding thin films inside a transmission electron microscope," *J. Mater. Res.*, vol. 20, no. 7, pp. 1769–1777, 2005.
[4] E. W. Wong, P. E. Sheehan, and C. M. Lieber, "Nanobeam mechanics: Elasticity, strength, and toughness of nanorods and nanotubes," *Science*, vol. 277, no. 5334, pp. 1971–1975, Sep. 1997.
[5] P. E. Marszalek, W. J. Greenleaf, H. Li, A. F. Oberhauser, and J. M. Fernandez, "Atomic force microscopy captures quantized plastic deformation in gold nanowires," *Proc. Nat. Acad. Sci. U.S.A.*, vol. 97, no. 12, pp. 6282–6286, Jun. 2000.
[6] M. F. Yu, O. Lourie, M. J. Dyer, K. Moloni, T. F. Kelly, and R. S. Ruoff, "Strength and breaking mechanism of multiwalled carbon nanotubes under tensile load," *Science*, vol. 287, no. 5453, pp. 637–640, Jan. 2000.
[7] C. L. Muhlstein, S. B. Brown, and R. O. Ritchie, "High-cycle fatigue of single-crystal silicon thin films," *J. Microelectromech. Syst.*, vol. 10, no. 4, pp. 593–600, Dec. 2001.
[8] H. Kahn, R. Ballarini, R. L. Mullen, and A. H. Heuer, "Electrostatically actuated failure of microfabricated polysilicon fracture mechanics specimens," *Proc. R. Soc. Lond. A, Math. Phys. Sci.*, vol. 455, no. 1990, pp. 3807–3823, Oct. 1999.
[9] Y. Zhu and H. D. Espinosa, "An electromechanical material testing system for *in situ* electron microscopy and applications," *Proc. Nat. Acad. Sci. U.S.A.*, vol. 102, no. 41, pp. 14 503–14 508, Oct. 2005.
[10] S. Eppell, B. Smith, H. Kahn, and R. Ballarini, "Nano measurements with micro-devices: Mechanical properties of hydrated collagen fibrils," *J. Roy. Soc. Interface*, vol. 3, no. 6, pp. 117–121, Feb. 2006.
[11] Y. Ganesan, Y. Lu, H. Lu, and J. Lou, "In situ mechanical characterization of one dimensional nanoscale building blocks using novel microfabricated devices," in *Proc. Conf. 8th IEEE-NANO*, 2008, pp. 783–786.
[12] Y. Lu, Y. Ganesan, and J. Lou, "A multi-step method for *in situ* mechanical characterization of 1-D nanostructures using a novel micromechanical device," *Exp. Mech.*, vol. 50, no. 1, pp. 47–54, Jan. 2010, DOI: 10.1007/s11340-009-9222-0.
[13] W. J. Meng and G. L. Eesley, "Growth and mechanical anisotropy of TiN thin films," *Thin Solid Films*, vol. 27, no. 1/2, pp. 108–116, Dec. 1995.

[14] *ASM Handbook*, vol. 2, 10th ed. Materials Park, OH: ASM, 1992, pp. 431–435.

[15] T. M. Whitney, P. C. Searson, J. S. Jiang, and C. L. Chien, "Fabrication and magnetic properties of arrays of metallic nanowires," *Science*, vol. 261, no. 5126, pp. 1316–1319, Sep. 1993.

[16] M. A. Meyers and K. K. Chawla, *Mechanical Behavior of Materials*. Upper Saddle River, NJ: Prentice-Hall, 1998, ch. 2.

[17] A. M. Howatson, P. G. Lund, and J. D. Todd, *Engineering Tables and Data*. Amsterdam, The Netherlands: Kluwer, 1991, p. 41.

Hao Lu received the B.S. degree in applied physics from the University of Science and Technology of China, Hefei, China. He is currently working toward the Ph.D. degree in physics in the Department of Mechanical Engineering and Materials Science, Rice University, Houston, TX.

His research interests include nanofriction, nanofluids, and the electrical and mechanical properties of nanomaterials.

Yogeeswaran Ganesan received the B.Tech. degree in chemical engineering from Anna University, Chennai, India. He is currently working toward the Ph.D. degree in materials science in the Department of Mechanical Engineering and Materials Science, Rice University, Houston, TX.

His research interests are in the field of *in situ* nanomechanics of carbon nanotubes and carbon-nanotube-reinforced nanocomposites.

Roberto Ballarini received the B.S. degree in civil engineering from The City College of New York, New York, NY, and the M.S. and Ph.D. degrees in civil engineering from Northwestern University, Evanston, IL.

He is the James L. Record Professor and Head of the Department of Civil Engineering, University of Minnesota, Minneapolis. His research interests include the mechanics of fracture and fatigue of materials and structures, with current focus on microelectromechanical systems, biological tissues, and carbon nanotubes.

Yang Lu received the B.S. degree in physics (microelectronics) from Nanjing University, Nanjing, China, in 2004, and the M.S. degree in materials engineering from New Mexico Tech, Socorro, in 2006. He is currently working toward the Ph.D. degree in mechanical engineering and materials science in the Department of Mechanical Engineering and Materials Science, Rice University, Houston, TX.

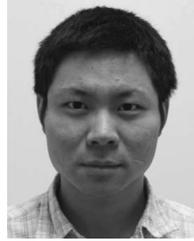His current research focuses on *in situ* nanomechanical characterization and integration of metallic nanowires.

Mr. Lu was a recipient of a Jack F. Pollard Endowed Fellowship in Engineering for 2008–2009 and an NSF–Sandia National Institute for Nano-Engineering Student Fellowship for 2009–2010.

Jun Lou received the B.S. degree in materials science and engineering from Tsinghua University, Beijing, China, the M.S. degree in materials science from The Ohio State University, Columbus, and the Ph.D. degree in materials science from Princeton University, Princeton, NJ.

He is currently an Assistant Professor in the Department of Mechanical Engineering and Materials Science, Rice University, Houston, TX. His research interests include nanomaterials synthesis, nanomechanical characterization, and nanodevice fabrication for energy and biomedical applications.

Dr. Lou was a recipient of an Air Force Young Investigator Award and the Oak Ridge Associated Universities Ralph E. Powe Junior Faculty Enhancement Award.

Cheng Peng received the B.S. degree in theoretical and applied mechanics and the M.S. degree in general mechanics and mechanical foundation from Fudan University, Shanghai, China. He is currently working toward the Ph.D. degree in mechanical engineering and materials science in the Department of Mechanical Engineering and Materials Science, Rice University, Houston, TX.

His research interests include fracture and fatigue mechanisms of thin films, micro-/nanomechanical characterization, and micro-/nanodevice fabrication.